J. Fluid Mech. (1995), *vol.* 293, *pp.* 127–145

Marangoni instabilities in liquid mixtures with Soret effects

By S. W. JOO

Department of Mechanical Engineering, Wayne State University, Detroit, MI 48202, USA

(Received 31 August 1994)

The stability of a binary liquid mixture heated from above is analysed. The heat transfer is driven by the imposed temperature difference between the horizontal bottom plate and the ambient gas. The mass flux in the layer is induced by the Soret effect. The gravitational effects are ignored, and the instability is driven by solutocapillarity and retarded by thermocapillarity. The interface is allowed to deform, and both the small-wavenumber and the Pearson-type instabilities are studied. Oscillatory instability can exist when the thermocapillary is destabilizing and the solutocapillarity is stabilizing.

1. Introduction

A horizontal liquid layer heated from below can become unstable, and various convective states can develop from the quiescent conductive state. There are two different types of mechanisms that drive the instabilities: (i) buoyancy due to the adverse density gradients (the Rayleigh–Bénard instability) and (ii) shear stress induced by the surface-tension gradient at the liquid/gas interface (the Marangoni instability). The second type persists in the absence of gravity.

Pearson (1958) performed a linear stability analysis for layers with non-deformable top surfaces (infinite surface-tension limit) heated from below by a constant-temperature or a fixed-flux plate, and reported the critical Marangoni numbers for the thermocapillary instability. Scriven & Sternling (1963) allowed the surface to deform (finite surface tension), and showed that the conductive state always becomes unstable at zero wavenumber. Smith (1966) clarified this unrealistic effect of surface deformation by incorporating the stabilizing hydrostatic effect, and obtained non-zero critical Marangoni numbers for the instability. These early works have been followed by numerous extensions, including a recent study by Goussis & Kelly (1990). They showed that there are two different modes of thermocapillary instability, one reported by Pearson (1958) with $O(1)$ wavenumber and the other associated with long-wave surface deformations. For sufficiently thin layers with the constant-temperature bottom plate, the Pearson type does not exist. The instability requires surface deformation, and occurs at zero wavenumber.

If the layer is a mixture and subjected to a concentration gradient, analogous instabilities will occur due to the surface-tension variation with the local concentration change. Instabilities due to this solutocapillarity and the thermocapillarity can coexist and compete with each other, resulting in oscillatory convection. Castillo & Verlarde (1982), McTaggart (1983), Ho & Chang (1988), and Chen & Su (1992), among others, studied the onset of convection in double-diffusive layers, where constant temperature and concentration are prescribed on the bottom and constant heat- and mass-transfer coefficients are specified on the top surface. They performed a stability analysis and

obtained marginal states for both stationary and oscillatory instabilities. The oscillatory convection is predicted when the two capillary effects are opposing each other, and is preferred for certain range of parameters. They assumed that the free surface is non-deformable, and thus allowed only the Pearson-type instabilities. A fairly extensive review of free convection in fluid mixtures is given by Platten & Legros (1984).

Most boundary conditions commonly used for the concentration are not easily realizable in practice. For example, it is very hard to maintain the constant-concentration condition on the bottom, used in the aforementioned studies of double-diffusive layers. In the present study, we consider a double-diffusive layer with a zero-mass-flux condition on both top and bottom boundaries. The mass flux in the fluid interior is then induced by local temperature gradients. This thermodiffusion of mass, so called the Soret effect, is non-trivial for some liquid mixtures, such as water/ethanol solution, and is well understood through non-equilibrium thermodynamics (see Landau & Lifshitz 1959; de Groot & Mazur 1962). Useful information, including the measurement of the Soret coefficient, can be found in the works of Platten & Legros (1984), Behringer (1985), Kolodner, Williams & Moe (1988), Van Vaerenberg, Colinet & Legros (1990), Cross & Hohenberg (1993), and the references therein. A stability analysis of fluid mixtures with the Soret effect for a rigid, low-heat-conducting surface has been reported by Castillo & Velarde (1978) for a few limiting cases.

We allow the free surface to deform, and thus capture the long-wave mode of capillary instability as well as the Pearson type. With the particular application in mind of freeze coating or casting of liquid mixtures (Kuiken 1977), where the liquid layer is frozen from below, we consider a liquid mixture heated from above. We formulate the problem in §2, and perform a linear stability analysis in §3. The results are summarized in §4, along with a method for studying the nonlinear development of the instabilities.

2. Basic state

We consider a binary liquid mixture of density ρ, viscosity μ, and thermal diffusivity κ on a rigid plate as shown in figure 1. The liquid layer is bounded above by a passive gas of ambient temperature T_∞, and is laterally unbounded. The temperature of the bottom plate is maintained at a constant value T_B, and the temperature difference $\Delta T(=T_\infty - T_B)$ induces the heat transfer across the liquid layer.

In a Cartesian coordinate system (x, y) fixed on the bottom plate, with y directed vertically upward into the liquid, the fluid motion in the layer is described by the continuity equation,

$$u_x + v_y = 0, \tag{1}$$

and the two components of the momentum equation,

$$(1/P)(u_t + uu_x + vu_y) = -p_x + \nabla^2 u, \tag{2}$$

$$(1/P)(v_t + uv_x + vv_y) = -p_y + \nabla^2 v, \tag{3}$$

where $\nabla^2 = \partial^2/\partial x^2 + \partial^2/\partial y^2$ and the Prandtl number

$$P = \nu/\kappa.$$

Here, the spatial variables (x, y), temporal variable t, velocity (u, v), and pressure p are, respectively, measured in units of the mean layer thickness d, thermal diffusion time d^2/κ, thermal diffusion speed κ/d, and $\mu\kappa/d^2$.

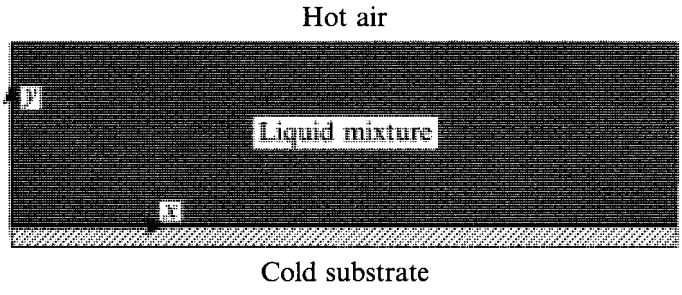

FIGURE 1. Liquid mixtures heated from above.

The heat transfer in the liquid layer is governed by the energy equation

$$T_t + uT_x + vT_y = \nabla^2 T, \tag{4}$$

where the temperature T is scaled by ΔT.

The mass transfer is described by

$$c_t + uc_x + vc_y = L\nabla^2(c + \Phi T), \tag{5}$$

where $c(x, y, t)$ is the solute concentration in the mixture and the inverse Lewis number L is the ratio of the mass diffusivity D to the thermal diffusivity:

$$L = D/\kappa.$$

Equation (5) shows that the diffusion of solute is induced not only by the concentration gradient but also by the temperature gradient. The extent of the thermal inducement of the concentration diffusion, namely the Soret effect, depends, in general, on the local concentration and temperature, but here it is measured by the parameter†

$$\Phi = k_T \Delta T / T_0,$$

where k_T is the thermodiffusion ratio (experimentally accessible) and T_0 is a dimensional reference temperature which can be taken to be the average temperature of the basic state $T_0 = T_B + \Delta T\, Bi/2(1 + Bi)$ (see below). A detailed discussion on the derivation of (5) through the Oberbeck–Boussinesq approximation can be found in the work by Hort, Linz & Lucke (1992) (see also Landau & Lifschitz 1959 and Behringer 1985). In (4), a cross-coupling in the temperature field, namely the Dufour effect, could exist, but is usually insignificant for liquid mixtures, as mentioned by Cross & Hohenberg (1993).

The dimensional surface tension $\tilde{\sigma}$ at the liquid–gas interface varies with the local temperature and concentration. Here, we assume that it is a linear function of $\tilde{T}$ and $\tilde{c}$ with coefficients α and β, respectively:

$$\tilde{\sigma}(\tilde{T}, c) = \sigma_0 - \alpha(\tilde{T} - T_0) - \beta(c - c_0), \tag{6}$$

where the zero subscripts denote reference values. For most common fluids, the surface tension decreases with the temperature increase, so that α is positive, but β can be either positive or negative depending on the composition of the mixture.

† A common way of modelling the concentration dependency of the Soret effect is to use $S_0\, c(1-c)$ in place of Φ, where S_0 is the Soret number. Most liquid mixtures, however, do not follow this idealized behaviour. The present study thus simplifies it to a piecewise-constant approximation.

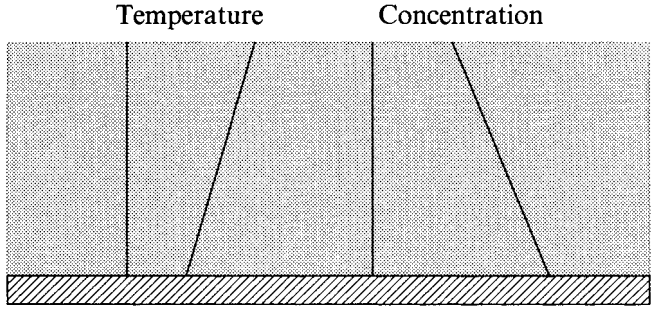

FIGURE 2. Purely conductive temperature and concentration profiles of the basic state.

The boundary condition for the normal stress at the interface then becomes

$$-p+\frac{2}{N^2}[u_x(\eta_x^2-1)-\eta_x(u_y+v_x)]=\frac{\Gamma_0}{N^3}[1-C_T(T-T^0)-C_s(c-c_0)]\eta_{xx} \quad \text{at} \quad y=1+\eta, \tag{7}$$

where $T^0 = T_0/\Delta T$ and $\eta(x, y, t)$ is the local deflection of the interface from its mean location $y = 1$. Here,

$$N=(1+\eta_x^2)^{1/2},$$

the non-dimensional mean surface tension

$$\Gamma_0=\sigma_0 d/\mu\kappa,$$

the thermal capillary number $C_T = \alpha\Delta T/\sigma_0$, and the solutal capillary number $C_s = \beta/\sigma_0$. The reciprocal of Γ_0 is sometimes called as the crispation number.

The location of the interface $y = 1+\eta$ is determined by introducing the kinematic condition

$$\eta_t = v+u\eta_x \quad \text{at} \quad y=1+\eta, \tag{8}$$

which states that the interface is a material surface.

The shear stress at the interface is induced by the surface-tension gradients along the surface. Using (6), we obtain

$$(u_y+v_x)(1-\eta_x^2)-4u_x\eta_x=-N[\bar{M}_T(T_x+\eta_x T_y)+\bar{M}_s(c_x+\eta_x c_y)] \quad \text{at} \quad y=1+\eta, \tag{9}$$

where $$\bar{M}_T = d\alpha\Delta T/(\mu\kappa) \quad \text{and} \quad \bar{M}_s = d\beta c_0/(\mu\kappa).$$

The parameters $\bar{M}_T$ and $\bar{M}_s$ are proportional to the thermal and solutal Marangoni numbers, which will be defined later.

The heat flux across the interface depends on the convective heat exchange with the gas phase, which is collectively approximated by the heat transfer coefficient h. The thermal boundary condition then is

$$\frac{T_y-\eta_x T_x}{N}+Bi(T-T^\infty)=0 \quad \text{at} \quad y=1+\eta, \tag{10}$$

where the Biot number

$$Bi = hd/\tilde{k},$$

$\tilde{k}$ is the heat conductivity of the mixture, and $T^\infty = T_\infty/\Delta T$.

The mixture is non-volatile, and so the mass flux across the interface is zero, which gives

$$c_y - \eta_x c_x + \Phi(T_y - \eta_x T_x) = 0 \quad \text{at} \quad y = 1 + \eta. \tag{11}$$

On the bottom plate, the velocity, the scaled temperature, and the mass flux all vanish, so that

$$u = v = T = c_y + \Phi T_y = 0 \quad \text{at} \quad y = 0. \tag{12}$$

One set of solutions of interest to the system (2)–(12) represents a hydrodynamically quiescent state, where the fluid is at rest and the heat and mass transfer are purely diffusive. In this case

$$\bar{u} = \bar{v} = \bar{p} = \bar{\eta} = 0, \tag{13}$$

$$\bar{T}(y) = \frac{Bi}{1 + Bi} y + T^B, \tag{14}$$

where $T^B = T_B/\Delta T$, and

$$\bar{c}(y) = \frac{\Phi Bi}{1 + Bi}(\tfrac{1}{2} - y) + c_0, \tag{15}$$

where the overbar represents the basic state. In (15),

$$c_0 = \int_0^1 \bar{c}(y)\,\mathrm{d}y$$

is the mean concentration of the solute.

The temperature and solute concentration profiles of the basic state are illustrated in figure 2. The temperature is T_B on the bottom and increases linearly to $Bi/(1 + Bi) + T^B$ at the interface. If $Bi \to 0$, the heat flux across the free surface vanishes, and the temperature gradient in the liquid layer disappears. Therefore, for the present analysis to be of any interest, the heat transfer coefficient at the liquid/gas interface should be non-zero, and the thermal conductivity of the mixture should be finite. If $Bi \to \infty$, the free surface behaves like a perfect conductor, and so the surface temperature becomes that of the ambient gas. The solute concentration also varies linearly, but its gradient depends on the sense of the parameter Φ. If $\Phi > 0$ (or < 0), the concentration decreases (or increases) vertically upward. As $\Phi \to 0$, the Soret effect disappears, and so the concentration becomes uniform.

The layers heated from *below* can be recovered by replacing the temperature scale ΔT with $-\Delta T$. This changes $Bi/(1 + Bi)$ into $-Bi/(1 + Bi)$ with other parameters and variables unaffected.

3. Linear stability analysis

It is expected that the conductive basic state (13)–(15) ceases to persist if the temperature gradient exceeds a certain critical value. Marangoni instabilities induce fluid flow, and various convective states set in. When the layer is cooled from below ($\Delta T > 0$) and the surface tension decreases with temperature ($\alpha > 0$) as usual, so that $\bar{M}_T$ is positive, the thermocapillarity is stabilizing. The solutocapillarity, however, can be destabilizing if $\Phi \bar{M}_s$ is positive. In this section, we quantify this Marangoni instability through linear stability analysis, and study the competition between the two capillary effects.

We consider disturbances of arbitrary horizontal wavenumber k and small amplitude δ superimposed on the basic state, and write the solutions of the full system as

$$\left.\begin{aligned} v &= \delta\, e^{\sigma t} e^{ikx} V(y), \\ T &= \bar{T} + \delta\, e^{\sigma t} e^{ikx} \theta(y), \\ c &= \bar{c} + \delta\, e^{\sigma t} e^{ikx} S(y), \\ \eta &= \delta\, e^{\sigma t} e^{ikx} \eta_0, \\ &\vdots \end{aligned}\right\} \tag{16}$$

where σ represents the complex growth rate of the disturbances. The capillary numbers C_T and C_s are usually very small, and will be set to zero in the analysis while the other parameters are set to be of order unity.

If we substitute these into the governing system (2)–(5) with the boundary conditions (7)–(12) and linearize in δ, we obtain, for the fluid flow,

$$V^{iv} - \left(2k^2 + \frac{\sigma}{P}\right) V'' + k^2 \left(k^2 + \frac{\sigma}{P}\right) V = 0 \tag{17}$$

with the boundary conditions

$$V(0) = V'(0) = 0, \tag{18}$$

$$k^4 V(1) - \frac{\sigma}{\Gamma_0}\left[V'''(1) - \left(3k^2 + \frac{\sigma}{P}\right) V'(1)\right] = 0, \tag{19}$$

$$V''(1) + k^2[\bar{M}_T \theta(1) + \bar{M}_s S(1)] + k^2 V(1) + \frac{Bi}{1+Bi} \frac{\bar{M}_T - \Phi \bar{M}_s}{\Gamma_0 k^2} [V'''(1) - (3k^2 + \sigma) V'(1)] = 0, \tag{20}$$

where the prime denotes differentiation with respect to y. The fluid-flow problem is coupled with the heat and mass transfer through the shear-stress condition (20). For the heat transfer we get

$$\theta'' - (k^2 + \sigma)\theta = \frac{Bi}{1+Bi} V \tag{21}$$

with

$$\theta(0) = \theta'(1) + Bi\theta(1) = 0, \tag{22}$$

and for the mass transfer

$$S'' - \left(k^2 + \frac{\sigma}{L}\right) S = -\Phi\left[\frac{Bi}{1+Bi}\left(1 + \frac{1}{L}\right) V - \sigma\theta\right] \tag{23}$$

with

$$S'(0) + \Phi\theta'(0) = S'(1) + \Phi\theta'(1) = 0. \tag{24}$$

The coefficient η_0 for the free-surface deformation is obtained as

$$\eta_0 = \frac{1}{\Gamma_0 k^4}[V'''(1) - (3k^2 + \sigma) V'(1)]. \tag{25}$$

The solutions for V, θ, and S are expanded in terms of hyperbolic sines and cosines,

and after some manipulations, as detailed in the Appendix, we obtain the characteristic equation

$$2z_0\sinh k-(1+z_0^2)\sinh kz_0-2z_1\cosh k+(1+z_0^2)z_1\cosh kz_0+\frac{1}{\sigma}\frac{Bi}{1+Bi}(\bar{M}_T-\Phi\bar{M}_s)$$

$$\times\left(-z_0\sinh k+\frac{P}{P-1}\sinh kz_0+z_2\sinh kz_p+z_1\cosh k-\frac{P}{P-1}z_1\cosh kz_0\right.$$

$$\left.+\frac{1}{P-1}z_1\cosh kz_p\right)+\frac{1}{\sigma}\frac{Bi}{1+Bi}\Phi\bar{M}_s\left[\frac{P}{(P-1)(P-L)}\sinh kz_0+\frac{z_2}{1-L}\sinh kz_p\right.$$

$$\left.-\frac{z_4}{z_s}\sinh z_s-\frac{P}{(P-1)(P-L)}z_1\cosh kz_0+\frac{z_1}{(P-1)(1-L)}\cosh kz_p+z_5\cosh kz_s\right]$$

$$+\frac{Bi}{1+Bi}\frac{\bar{M}_T-\Phi\bar{M}_s}{\Gamma_0 k}[(1+z_0^2)z_1\sinh k-2z_0z_1\sinh kz_0$$

$$-(1+z_0^2)z_0\cosh k+2z_0\cosh kz_0]=0, \tag{26}$$

where the z_i are defined in the Appendix.

3.1. *Stationary branch* ($\sigma=0$)

The stability bounds, beyond which instabilities develop without temporal oscillations, can be obtained by setting $\sigma=0$. As shown in the Appendix, the characteristic equation for this stationary instability is reduced to

$$8k^2\sinh k(k-\sinh k\cosh k)+(M_T-LM_s)\frac{k^4\sinh k\cosh k-k\sinh^4 k}{k\cosh k+Bi\sinh k}$$

$$-M_s(k^3\sinh k-k^2\cosh k+2k\sinh k-\sinh^2 k\cosh k)-\frac{M_T-LM_s}{\Gamma_0}8k^3\sinh k=0. \tag{27}$$

Considering the temperature profile (14) and the concentration profile (15) of the basic state, we notice that

$$M_T\equiv\frac{Bi}{1+Bi}\bar{M}_T=\frac{hd}{hd+\tilde{k}}\frac{\alpha d\Delta T}{\mu\kappa}\quad\text{and}\quad M_s\equiv\frac{Bi}{1+Bi}\frac{\Phi}{L}\bar{M}_s=\frac{hd}{hd+\tilde{k}}\frac{\beta d\Delta Tc_0k_T}{\mu DT_0}$$

are the thermal and solutal Marangoni numbers, respectively.†

The last term in (27) describes the effects of free-surface deformations. In the large-surface-tension limit, $\Gamma_0\to\infty$, the effects of surface deformations vanish. The characteristic equation (27) then is reduced to that for a non-deformable surface. In this case, the following comparisons can be made to the analysis performed by Pearson

† In experiments M_T is often controlled by changing ΔT. If one wishes to measure the solutal Marangoni effect independent of ΔT, one can rewrite $M_s=\psi M_T/L$ and use ψ as an alternative parameter, where the separation ratio $\psi=\beta k_T c_0/\alpha T_0$.

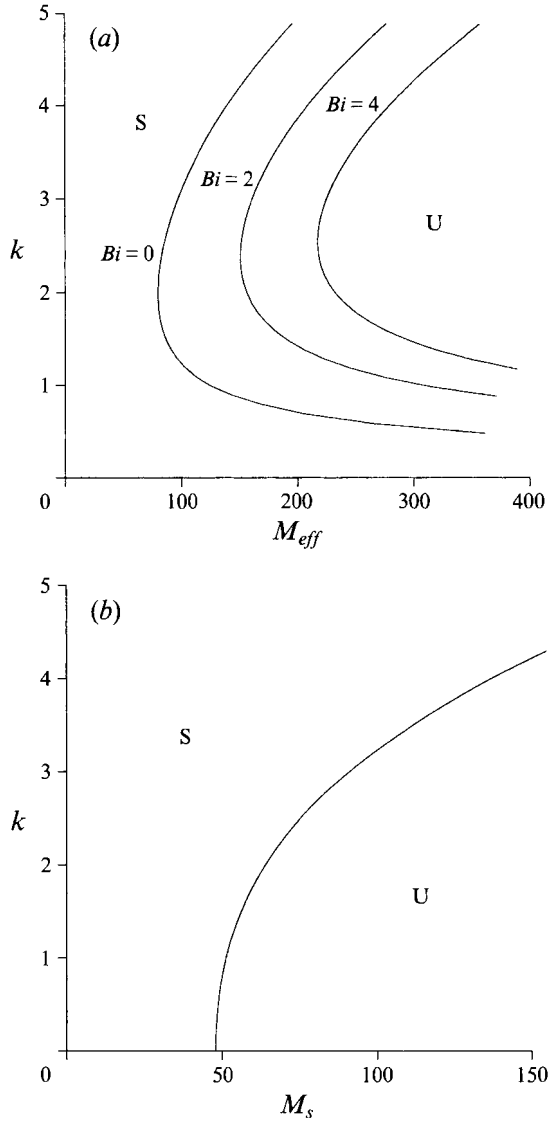

FIGURE 3. Stability diagram for a non-deformable surface analogous to the Pearson's (1958) case of (*a*) a conducting and (*b*) insulating bottom boundary. S denotes stable and U unstable.

(1958) for pure thermocapillary instability. If $M_s \to 0$ while $LM_s = O(1)$, we recover his 'conducting case', with his thermal Marangoni number replaced by an effective Marangoni number

$$M_{eff} \equiv -M_T + LM_s.$$

In this limit, the disturbances for the solute and the temperature are related by $S(y) = -\Phi\theta(y)$ (see (21) and (23) for $k = 0$). If $L = O(1)$ with $M_s \to 0$, we get $M_{eff} = -M_T$. The minus sign in front of M_T occurs because the sign of the temperature difference in the conductive state is opposite to that in Pearson's case, where the liquid layer is heated from below. In the present case, the thermocapillary (with $M_T > 0$) stabilizes the flow while the solutocapillarity (with $M_s > 0$) destabilizes, as can be deduced from the stability diagram in figure 3(*a*). If $M_T \to 0$ and $L \to 0$, then $\bar{M}_{eff} \to 0$ and Pearson's

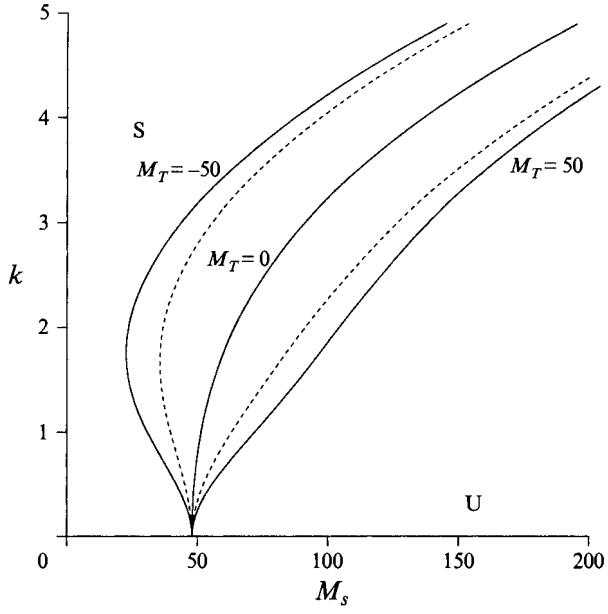

FIGURE 4. The thermocapillary effects on the solutocapillary instability when the surface is non-deformable and $L = Bi = 0$. The broken lines are for $Bi > 0$.

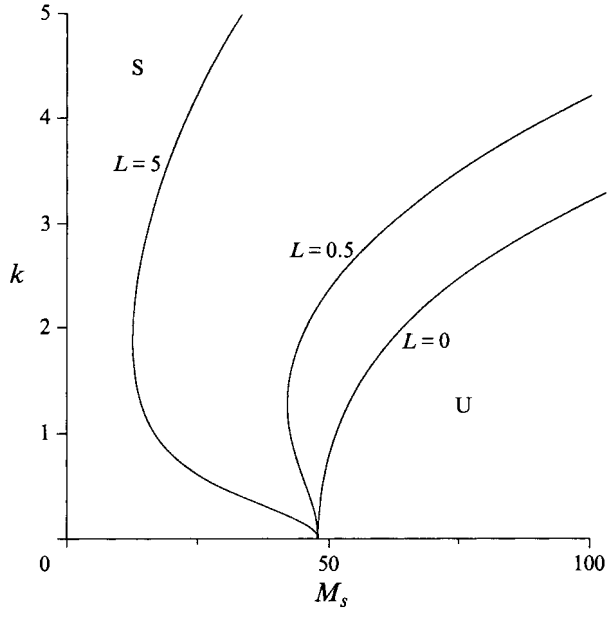

FIGURE 5. Pure solutocapillary instability for a non-deformable surface when $Bi = 0$.

'insulating case' is recovered, with his thermal Marangoni number replaced by the solutal Marangoni number M_s and his Biot number set to zero. The corresponding stability diagram is shown in figure 3(*b*). It is noteworthy that the pure solutocapillarity instability occurs in the form of long waves, which is often referred to as 'zero-wavenumber' instability.

Figure 4 shows the stationary branches when both the thermo- and solutocapillarity

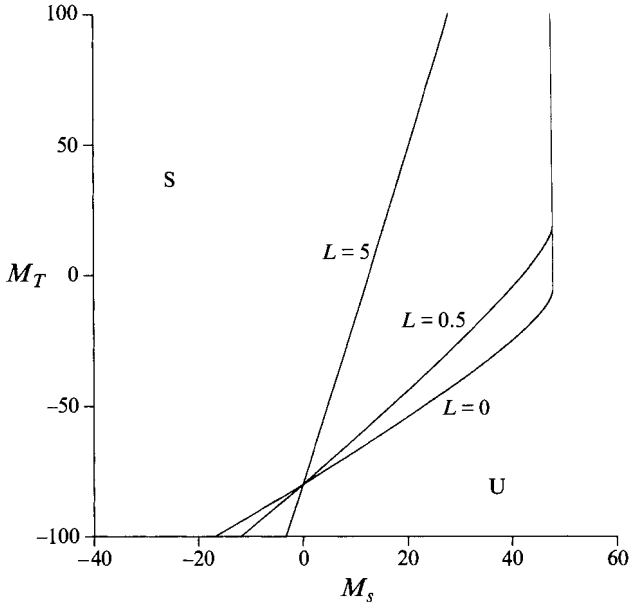

FIGURE 6. Stability diagram for a non-deformable surface when $Bi = 0$. Stable region does not exist for $M_s > 48$.

are present. The branch for $M_T = 0$ is identical to that in figure 3(*b*) (Pearson's insulating case), and intersects the horizontal axis vertically at $M_s = 48$. If $M_T > 0$ (or $M_T < 0$) the thermocapillarity stabilizes (or destablizes) the flow, and so the stable (or unstable) region expands. For sufficiently large negative values of M_T (strong thermocapillary instability), the branch crosses the vertical axis, so that instability occurs even for negative M_s. For a non-deformable surface ($\Gamma \to \infty$) long disturbances (small k) are not affected by the thermocapillarity of the 'conducting' type, so that the intersection with the horizontal axis stays at $M_s = 48$ regardless of the values of M_T and Bi. The two broken lines show the effects of the heat transfer coefficient at the gas/liquid interface. As Bi increases, the thermocapillary effect diminishes and the branches move toward that for $M_T = 0$ until they coincide for $Bi \to \infty$, as can be expected from (27).

A non-zero inverse Lewis number L enhances the solute convection, and thus destabilizes the flow. Figure 5 displays the stationary branches for three different L. As L increases, the unstable region expands. As in the thermocapillary destabilization, disturbances of small wavenumbers are not affected, so that all branches start at $M_s = 48$ at $k = 0$. However, contrary to the thermocapillary destabilization, the branch never crosses the vertical axis; there is no instability for negative M_s.

Figure 6 shows three stationary branches in the (M_s, M_T)-plane for a non-deformable interface. When $L = 0$, the branch is vertical for $M_T > 0$. The 'zero-wavenumber' instability persists with the critical Marangoni number of 48, as shown in figure 4. As M_T decreases further, the thermocapillary destabilization makes the branch bend with decreasing slope until it becomes almost horizontal (not shown in the figure) for $M_T \to -\infty$. When $L > 0$, the critical solutal Marangoni number corresponds to $O(1)$ wavenumber (no longer the 'zero-wavenumber' instability) as shown in figure 5, and becomes sensitive to M_T. The bending, therefore, occurs for $M_T > 0$, and the rate of decrease in slope is smaller. Regardless of L, all branches pass

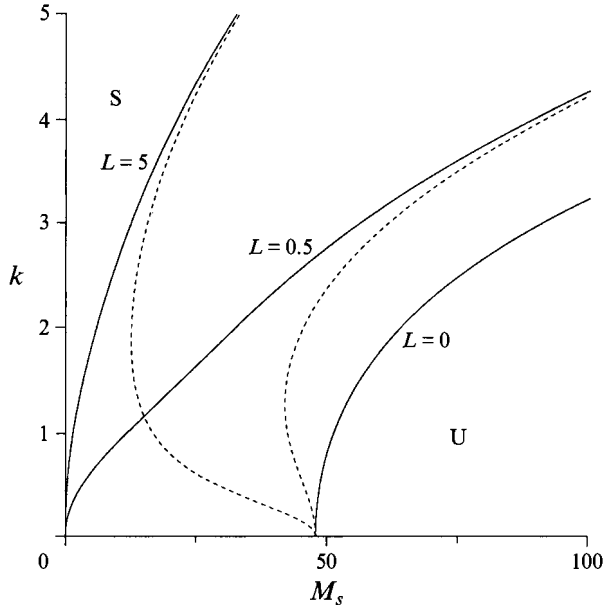

FIGURE 7. Pure solutocapillary instability for a deformable surface when $Bi = 0$ and $\Gamma_0 = 10$. The broken lines are the corresponding branches for a non-deformable surface.

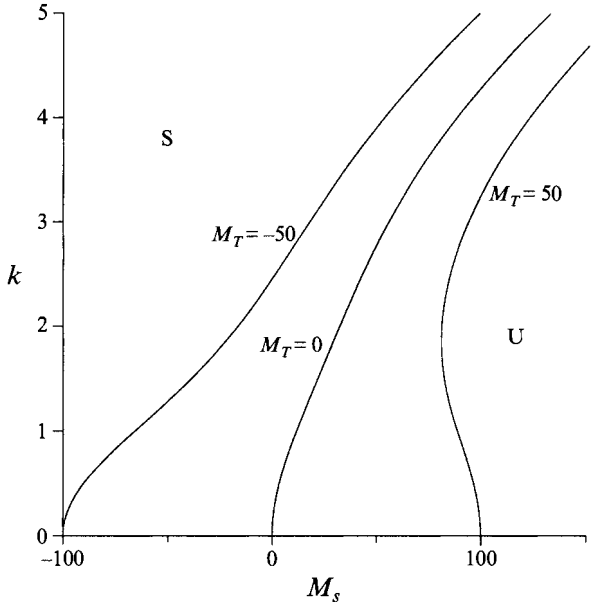

FIGURE 8. The thermocapillary effects on the solutocapillary instability when the surface is deformable, $Bi = 0$, $L = 0.5$ and $\Gamma_0 = 10$.

through (0, 79.6), a point for pure thermocapillary instability. The thermal Marangoni number M_T at this point is in agreement with the critical Marangoni number for the 'conducting' case, or the branch for $Bi = 0$ in figure 3(*a*).

The effect of surface deformation can be studied by allowing a finite value of Γ_0. As tabulated for a few pure liquid layers by Smith (1966, table 1), the values for Γ_0 are

usually very large for most common fluids, although for the highly viscous silicone oil Γ_0 is near order unity.

When both M_T and L are zero, the surface deformation has no effect on the stability of the flow, and so figure 3(*b*) is unaffected by variations of Γ_0. This can be easily deduced from (27) with $M_T = L = 0$. Figure 7 shows the stationary branches for three different values of L with $M_T = 0$ and $\Gamma_0 = 10$. The broken lines indicate the corresponding branches with no surface deformation ($\Gamma_0 \to \infty$). As expected, the lines for $L = 0$ overlap each other. For non-zero values of L, the intersection point with the horizontal axis is shifted to the origin. The critical solutal Marangoni number $(M_s)_c$ is always zero, and the zero-wavenumber instability occurs. For large k, the effect of surface deformation diminishes, and all branches approach those for $\Gamma_0 \to \infty$.

The cases shown in figure 7 for $L \neq 0$ are analogous to those reported by Scriven & Sternling (1963, figure 2) for thermocapillarity of the 'insulating' type. However, they excluded the area near the origin in their stability diagram, and failed to notice that $(M_s)_c$ is zero rather than $-\infty$ when the heat flux (solute flux in our case) is zero at the surface. The fact that the branch never crosses the vertical axis for $M_T \geqslant 0$ makes sense.

In most experiments, $(M_s)_c$ will be positive owing to the hydrostatic stabilization. As discussed by Smith (1966) and by Scanlon & Segel (1967), the effect of gravity can be incorporated through the normal-stress condition (7). A term proportional to $-\eta We$ would be added to the right-hand side of the equation, where $We = \rho g d^2/\sigma_0$ is the Weber number. In the characteristic equations above, Γ_0 would be replaced by

$$\Gamma = \Gamma_0(1 + We/k^2).$$

The small-wavenumber behaviour of the stationary branch in the (k, M_s)-plane can be obtained by expanding (27) for small k and solving for M_s, which gives

$$M_s = \frac{48 + 72M_T/(\Gamma_0 We)}{1 + 72L/(\Gamma_0 We)} + O(k^2). \tag{28}$$

In the absence of gravity ($We = 0$), we get $(M_s)_c = M_T/L$, which is consistent with figure 7 for $M_T = 0$ and figure 8 below for $M_T \neq 0$. In the rigid-surface limit, $\Gamma_0 We \to \infty$ and (28) reduces to $M_s = 48 + O(k^2)$.

Figure 8 shows three stationary branches for $M_T = -50$, 0, and 50 with $L = 0.5$ and $\Gamma_0 = 10$. The values for $(M_s)_c$ are, respectively, -100, 0, 100, consistent with (28). All branches show zero-wavenumber instability.

In figure 9, three stationary branches are drawn in the (M_s, M_T)-plane for different values of Γ_0 with $L = 0.5$. The branch with no label corresponds to the non-deformable surface ($\Gamma_0 \to \infty$). As explained for figure 6, the branch cannot cross the $M_s = 48$ line. For M_T somewhat larger than zero, the zero-wavenumber instability occurs, and the stability bounds are fixed at $M_s = 48$. When the surface is deformable, the branch crosses the $M_s = 48$ line. As seen figure 8, finite-wavenumber instability occurs for $M_s > 48$. The thermocapillary stabilization is more effective in this range, and so the stable region expands with the decrease of the mean surface tension. For $M_s < 48$, zero wavenumber occurs if the surface is deformable. Since the critical value for the instability is given by $(M_s)_c = M_T/L$, the branch is a straight line passing through the origin ($M_T = M_s = 0$) with slope L regardless of the value of Γ_0. In this range, the surface deformation further destabilizes the flow.

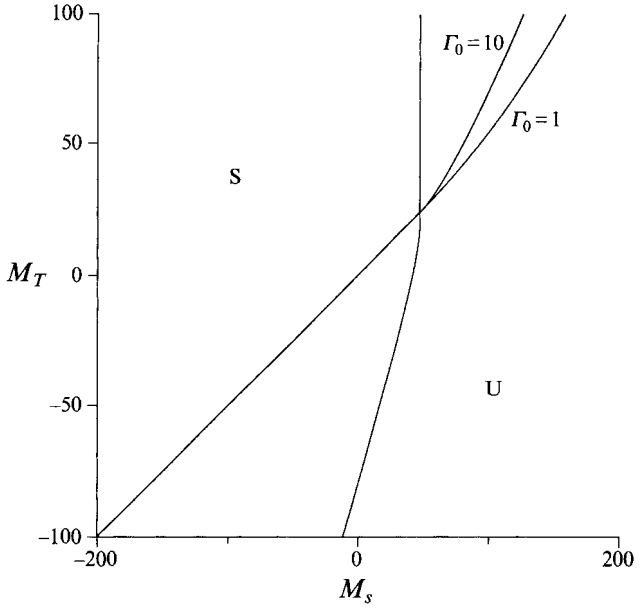

FIGURE 9. Stability diagram for a deformable surface when $Bi = 0$ and $L = 0.5$. For a finite Γ_0, the stable region penetrates beyond $M_s = 48$, so that there is additional stabilization and destabilization due to the long-wave mode, which is absent for the non-deformable surface.

3.2. *Oscillatory branch*

The threshold for the Hopf bifurcation beyond which the disturbances grow with temporal oscillations can be obtained from (26) by setting $\sigma = i\omega_H$, where ω_H is the Hopf frequency. The characteristic equation (26) then takes the form

$$f(k, \omega_H, \boldsymbol{P}) = 0, \tag{29}$$

where f is a complex function and $\boldsymbol{P}$ is the parameter vector. Given the wavenumber k and all the parameter values except M_s, we iterate on ω_H and M_s until they satisfy the real and imaginary parts of (29) simultaneously. Oscillatory branches are obtained by extending the solution for M_s for different values of k or other parameters.

In figure 10(*a*), oscillatory branches (indicated by broken lines) are shown in the (k, M_s)-plane for $M_T = -50$, $L = 0.5$, $\Gamma_0 = 10$, and $Bi = 0$. The solid line indicates the stationary branch for these parameters. The stationary branch does not depend on the Prandtl number. For the oscillatory branch, however, P must be specified: three different values are chosen. There is little change from the branch for $P = 5$ for larger values of P, so that $P = 5$ can be considered as a representative of large Prandtl number. For all Prandtl numbers, the oscillatory branch starts at $M_s \approx 147$ on the horizontal axis and terminates on the stationary branch. The oscillatory instability is enhanced as the Prandtl number decreases. The temporal oscillation seems to occur owing to the competition between the destabilizing thermocapillarity and the stabilizing solutocapillarity. The critical solutal Marangoni number $(M_s)_c$ for the oscillatory instability is always smaller than that for the stationary instability. Figure 10(*b*) shows the Hopf frequency ω_H of the branch $P = 5$. The Hopf frequency is defined for $-147 < M_s < -23.6$, where the branch $P = 5$ exists. It increases from zero at $M_s = -147$, and reaches a maximum near the midpoint before it decreases to zero at $M_s = -23.6$.

It is noteworthy that the oscillatory branch is confined to the $M_s < 0$ region. It does

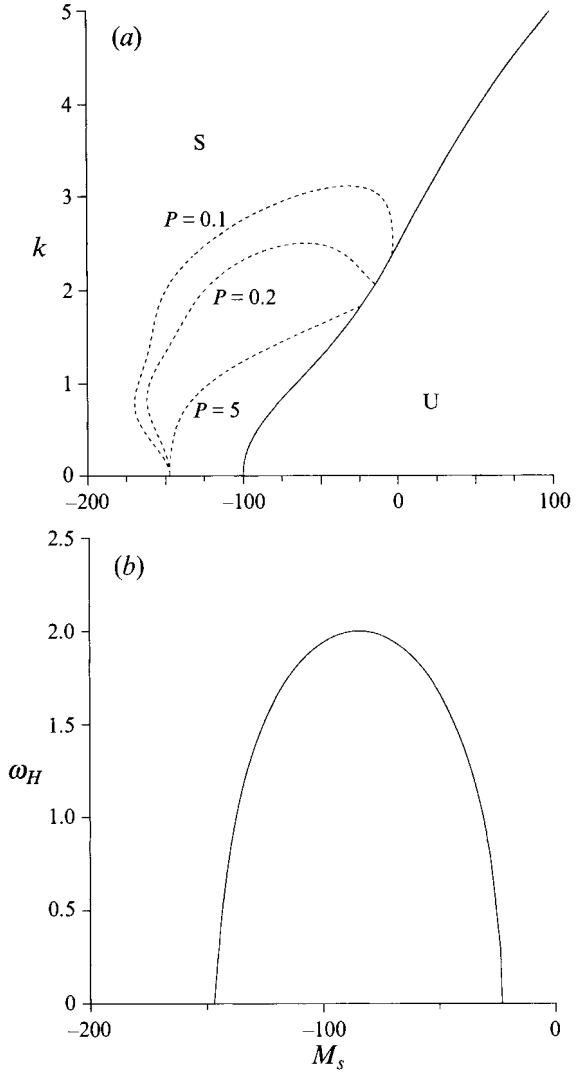

FIGURE 10. (*a*) Oscillatory branches (broken lines) when $Bi = 0$, $M_T = -50$, $L = 0.5$, and $\Gamma_0 = 10$. (*b*) The Hopf frequency ω_H for $P = 5$.

not cross the $M_s = 0$ line. Therefore, stabilizing thermocapillarity ($M_T > 0$) coupled with destabilizing solutocapillarity ($M_s > 0$) does not generate oscillations. In water–alcohol mixtures, the Soret coefficient, or Φ in the present analysis, changes its sense to negative values for sufficiently high alcohol concentration. Therefore, if one wishes to realize the oscillatory instability in these mixtures, one must heat them from below ($\Delta T < 0$ and thus $M_T < 0$) and use dilute solutions ($\Phi > 0$ and thus $M_s < 0$). For a non-deformable surface ($\Gamma_0 \to \infty$), the intersection point of the stationary branch on the horizontal axis moves to a positive value $M_s = 48$. Thus, we have not found any oscillations for layers with non-deformable surfaces.

In figure 11(*a*), three oscillatory branches and the corresponding stationary branch are shown for the same parameter values as those for figure 10 except that $\Gamma_0 = 1000$. All three Prandtl numbers give almost the same oscillatory branches, so that the three broken lines look collapsed into one. As the surface tension increases, the free surface

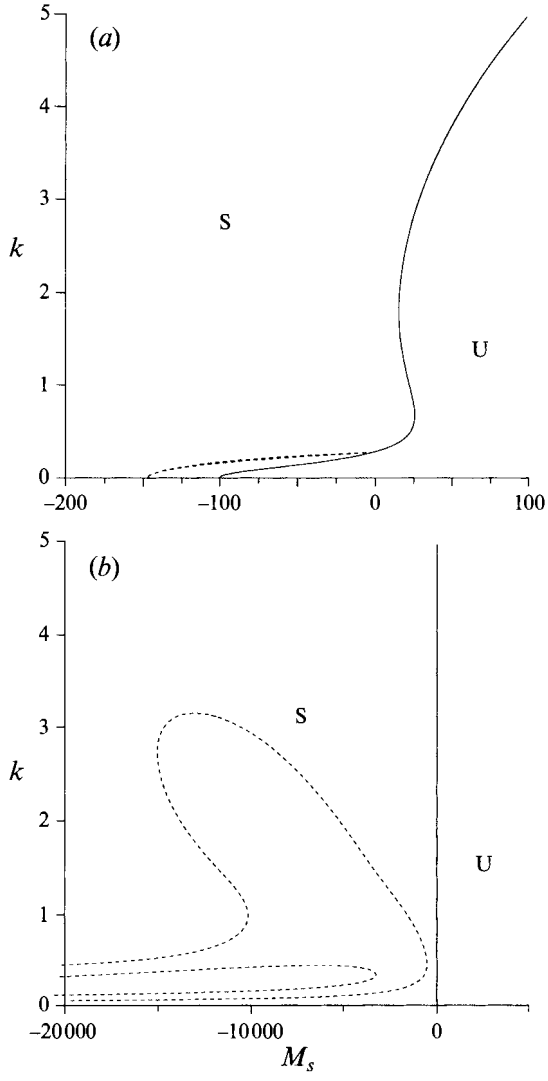

FIGURE 11. (*a*) Oscillatory branches (broken lines) when $Bi = 0$, $M_T = -50$, $L = 0.5$, and $\Gamma_0 = 1000$. (*b*) Additional branches for $P = 0.2$.

behaves more like a rigid surface. The region for oscillatory instability decreases accordingly, and seems to disappear as $\Gamma_0 \to \infty$. This explains why we could not find oscillations for the non-deformable surface. For layers with very small Prandtl numbers, isolated oscillatory branches are found for very large surface tension, as shown in figure 11 (*b*). These branches seem to extend toward $M_s = -\infty$. Liquid metals usually have small Prandtl numbers but their Soret effects are very small. In order to observe the isolated branches, extremely large temperature gradients may be required.

In figure 12, the oscillatory and stationary instability bounds are shown for $P = 5$, $L = 0.5$, and $L = 5$. The oscillatory instability exists when the thermocapillarity is destabilizing and the solutocapillarity is stabilizing, as explained above. The oscillatory branch, therefore, terminates on the stationary branch in the third quadrant of the (M_T, M_s)-plane. In the parameter ranges where the oscillatory instability can occur, it is preferred to the stationary mode. As is obvious from figures 10 and 11, the oscillatory

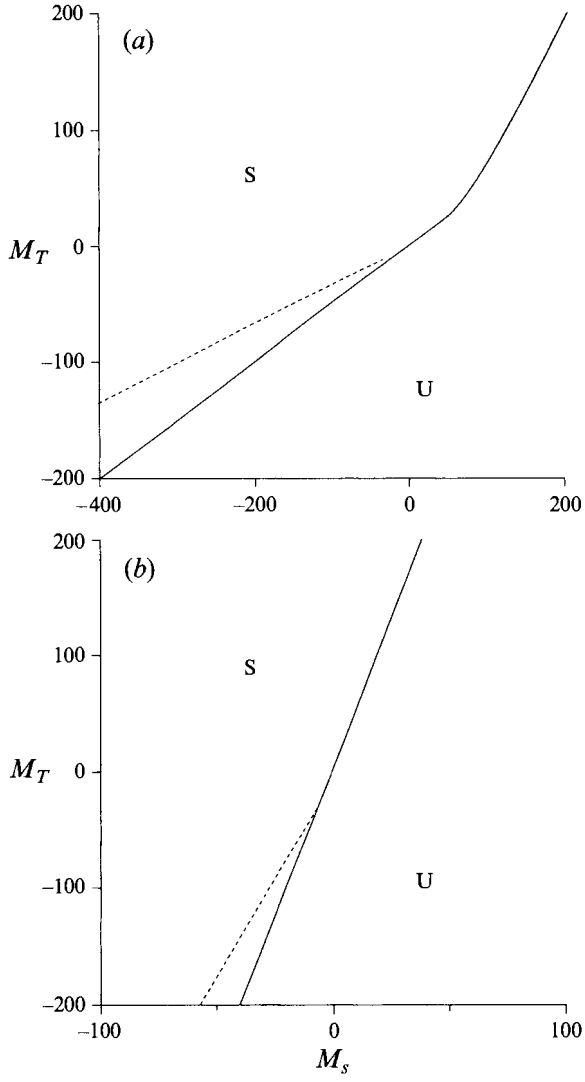

FIGURE 12. Oscillatory (broken lines) and stationary (solid lines) branches when $Bi = 0$ and (*a*) $L = 0.5$ and (*b*) $L = 5$.

instability for moderate and large Prandtl numbers occurs for small wavenumbers. The oscillatory branch in figure 12 thus corresponds to zero wavenumber. The stationary branch switches from zero-wavenumber to $O(1)$-wavenumber instabilities in the first quadrant. The critical solutal Marangoni numbers for the zero-wavenumber instabilities are proportional to the Lewis number $1/L$ for both oscillatory and stationary instabilities, so that the slopes of the branches in the third quadrant increase with L, as seen in figure 12(*b*).

4. Concluding remarks

A linear stability analysis is performed for a layer of binary liquid mixture heated from above. The gravitational effects, such as the buoyancy-driven convection, are ignored. The fluid motion is induced by the thermo- and solutocapillary effects. The

heat transfer across the liquid layer is driven by the imposed temperature gradient, whereas the mass transfer exists due to the Soret effect.

The quiescent state with purely conductive heat and mass transfer can become linearly unstable owing to the solutocapillarity. Since the layer is heated from above, the thermocapillarity stabilizes the flow for most common fluids, whose surface tension decreases with the temperature increase.

In the large-surface-tension limit (non-deformable surface), the solutocapillary instability is analogous to the thermocapillary instability reported by Pearson (1958) with the 'conducting' and the 'insulating' cases present simultaneously. Therefore, both the zero- and $O(1)$-wavenumber instabilities can occur depending upon the parameter values, as detailed in the previous section. For the non-deformable surface, the long-wave thermocapillary stabilization is absent (as discussed by Goussis & Kelly (1990), this mode requires surface deformation). The thermocapillary stabilization thus is not effective on the zero-wavenumber solutocapillary instability. Regardless of the thermal Marangoni number, the flow becomes always unstable if the solutal Marangoni number exceeds 48 (see figure 6).

For a deformable surface, there is competition between the long-wave mode of the thermocapillary stabilization and of the solutocapillary destabilization. Therefore, for most common fluids, the critical solutal Marangoni number is a positive number. The corresponding wavenumber at the onset is of $O(1)$ for sufficiently strong thermocapillary stabilization. The present results also clarify the stability bounds reported by Scriven & Sternling (1963) for an analogous problem.

For a deformable surface, the oscillatory instability is also found. It occurs when the thermocapillarity is destabilizing and the solutocapillarity is stabilizing. When a layer is heated from above and the interfacial tension decreases with temperature, only stationary convections are likely to occur.

The author is grateful to Professor Stephen H. Davis for his invaluable help throughout the present study. The author also thanks Dr Stefan Linz for helpful discussions. This work was supported in part by the US Department of Energy, Division of Basic Energy Sciences, through Grant No. DE FG02-86ER13641 and by the Institute for Manufacturing Research, Wayne State University.

Appendix. Derivation of the characteristic equation

The solution of (17) that satisfies the boundary conditions (18)–(19) is

$$V(y) = z_0 \sinh ky - \sinh kz_0 y - z_1 \cosh ky + z_1 \cosh kz_0, y \tag{A 1}$$

where

$$z_0 = (1+\sigma/Pk^2)^{1/2}$$

and

$$z_1 = \frac{z_0 \sinh k - \sinh kz_0 + (\sigma z_0/\Gamma_0 k)[(1+z_0^2)\cosh k - 2\cosh kz_0]}{(\cosh k - \cosh kz_0) + (\sigma/\Gamma_0 k)[(1+z_0^2)\sinh k - 2z_0 \sinh kz_0]}.$$

Here, an arbitrary constant factor is set to unit without loss of generality. The solution of (21) subject to the conditions (22) is

$$\theta(y) = \frac{1}{\sigma}\frac{Bi}{1+Bi}\left(-z_0 \sinh ky + \frac{P}{P-1}\sinh kz_0 y \right.$$

$$\left. + z_2 \sinh kz_p y + z_1 \cosh ky - \frac{P}{P-1} z_1 \cosh kz_0 y + \frac{1}{P-1} z_1 \cosh kz_p y\right), \tag{A 2}$$

where $$z_p = (1+\sigma/k^2)^{1/2}$$

and $$z_2 = \Big[(z_0 B_i - kz_1)\sinh k - \frac{P}{P-1}(Bi - kz_0 z_1)\sinh kz_0 - \frac{z_1}{P-1} \times (kz_p \sinh kz_p + Bi\cosh kz_p) + (kz_0 - z_1 Bi)\cosh k - \frac{P}{P-1} \times (kz_0 - Biz_1)\cosh kz_0\Big] / (Bi\sinh kz_p + kz_p \cosh kz_p).$$

From (23) and (24), we obtain

$$S(y) = \frac{\Phi}{\sigma}\frac{Bi}{1+Bi}\Big(z_0\sinh ky + z_3\sinh kz_0 y + \frac{L}{1-L}z_2\sinh kz_p y - \frac{z_4}{z_s}\sinh kz_s y - z_1\cosh ky - z_1 z_3\cosh kz_0 y + \frac{L}{(P-1)(1-L)}z_1\cosh kz_p y + z_5\cosh kz_s y\Big), \tag{A 3}$$

where

$$z_s = \Big(1+\frac{\sigma}{Lk^2}\Big)^{1/2}, \quad z_3 = \frac{P}{(P-1)(P-L)} - \frac{P}{P-1}, \quad z_4 = \Big[\frac{Pz_0}{(P-1)(P-L)} + \frac{z_2 z_p}{1-L}\Big],$$

$$z_5 = \frac{1}{z_s\sinh kz_s}\Big[\frac{Pz_0 z_1}{(P-1)(P-L)}\sinh kz_0 - \frac{z_1 z_p}{(P-1)(1-L)}\sinh kz_p - \frac{Pz_0}{(P-1)(P-L)}\cosh kz_0 - \frac{z_2 z_p}{1-L}\cosh kz_p + z_4\cosh kz_s\Big].$$

The characteristic equation (26) can be obtained by substituting the eigenvalues (A 1)–(A 3) into the shear-stress condition (20).

For stationary branches $\sigma \to 0$, in which case the eigenfunctions are

$$V(y) = \sinh ky + \frac{k\cosh k - \sinh k}{\sinh k} y\sinh ky - ky\cosh ky, \tag{A 4}$$

$$\theta(y) = \frac{1}{4}\frac{Bi}{1+Bi}\Big[\Big(z_6 - \frac{k\cosh k - \sinh k}{k^2\sinh k}y - y^2\Big) \times \sinh ky + \Big(3y + \frac{k\cosh k - \sinh k}{\sinh k}y^2\Big)\frac{\cosh ky}{k}\Big], \tag{A 5}$$

and

$$S(y) = \frac{\Phi}{4}\frac{Bi}{1+Bi}\Big(1+\frac{1}{L}\Big)\Big[\Big(-\frac{P}{P+Sc}z_6 + \frac{3}{k^2}\frac{Sc}{P+Sc} + \frac{k\cosh k - \sinh k}{k^2\sinh k}y + y^2\Big) \times \sinh ky + \Big(\frac{Sc}{P+Sc}\Big(\frac{k\cosh k - \sinh k}{k\sinh k}\Big)^2 - 3y - \frac{k\cosh k - \sinh k}{\sinh k}y^2\Big)\frac{\cosh ky}{k}\Big], \tag{A 6}$$

where

$$z_6 = -\frac{k^2\cosh^2 k + k\sinh k\cosh k + \sinh^2 k + Bi(k^2 + k\sinh k\cosh k + \sinh^2 k)}{k^2\sinh k\,(k\cosh k + Bi\sinh k)}.$$

The characteristic equation then is reduced to (27).

REFERENCES

BEHRINGER, R. P. 1985 Rayleigh–Bénard convection and turbulence in liquid helium. *Rev. Mod. Phys.* **65**, 657–687.

CASTILLO, J. L. & VERLARDE, M. G. 1978 Thermal diffusion and the Marangoni-Benard instability of a two-component fluid layer heated from below. *Phys. Lett.* **66A**, 489–491.

CASTILLO, J. L. & VELARDE, M. G. 1982 Buoyancy-thermocapillary instability: the role of interfacial deformation in one- and two-component fluid layers heated from below or above. *J. Fluid Mech.* **125**, 463–474.

CHEN, C. F. & SU, T. F. 1992 Effect of surface tension on the onset of convection in a double-diffusive layer. *Phys. Fluids* A **4**, 2360–2367.

CROSS, M. C. & HOHENBERG, P. C. 1993 Pattern formation outside of equilibrium. *Rev. Mod. Phys.* **65**, 851–1112.

GOUSSIS, D. A. & KELLY, R. E. 1990 On the thermocapillary instabilities in a liquid layer heated from below. *Intl J. Heat Mass Transfer* **33**, 2237–2245.

GROOT, S. R. DE & MAZUR, P. 1962 *Nonequilibrium Thermodynamics*. North Holland.

HO, K.-L. & CHANG, H.-C. 1988 On nonlinear doubly-diffusive Marangoni instability. *AIChE J.* **34**, 705–722.

HORT, W., LINZ, S. J. & LUCKE, M. 1992 Onset of convection in binary gas mixtures: the role of the Dufour effect. *Phys. Rev.* A **45**, 3737–3748.

KOLODNER, P., WILLIAMS, H. & MOE, C. 1988 Optical measurement of the Soret coefficient of ethanol/water solutions. *J. Chem. Phys.* **88**, 6512–6524.

KUIKEN, H. K. 1977 Solidification of a liquid on moving sheet. *Intl J. Heat Mass Transfer* **20**, 309–314.

LANDAU, L. D. & LIFSHITZ, E. M. 1959 *Hydrodynamics*. Pergamon.

MCTAGGERT, C. L. 1983 Convection driven by concentration and temperature-dependent surface tension. *J. Fluid Mech.* **134**, 301–310.

PEARSON, J. R. A. 1958 On convection cells induced by surface tension. *J. Fluid Mech.* **4**, 489–500.

PLATTEN, J. K. & LEGROS, J. C. 1984 *Convection in Liquids*, Chap. IX, pp. 567–675. Springer.

SCANLON, J. W. & SEGEL, L. A. 1967 Finite amplitude cellular convection induced by surface tension. *J. Fluid Mech.* **30**, 149–162.

SCRIVEN, L. E. & STERNLING, C. V. 1963 On cellular convection driven by surface-tension gradients: effects of mean surface tension and surface viscosity. *J. Fluid Mech.* **19**, 321–340.

SMITH, K. A. 1966 On convection instability induced by surface-tension gradients. *J. Fluid Mech.* **24**, 401–414.

VAN VAERENBERG, S., COLINET, P. & LEGROS, J. C. 1990 *The Role of the Soret Effect on Marangoni–Bernard Stability*. Springer.